INSTITUTE OF PHYSICS PUBLISHING JOURNAL OF PHYSICS D: APPLIED PHYSICS

J. Phys. D: Appl. Phys. **34** (2001) 1100–1109 www.iop.org/Journals/jd PII: S0022-3727(01)19370-8

# Electronegativity of low-pressure high-density oxygen discharges

**J T Gudmundsson[1], I G Kouznetsov[2,3], K K Patel[2,4] and M A Lieberman[2]**

[1] Science Institute, University of Iceland, Dunhaga 3, IS-107 Reykjavík, Iceland
[2] Department of Electrical Engineering and Computer Sciences, University of California, Berkeley, CA 94720, USA

Received 27 November 2000

**Abstract**

We use a global (volume averaged) model to study the presence of negative ions and metastable species in low-pressure high-density oxygen discharges. We find the negative oxygen ion $O^-$ to be the dominant negative ion in the discharge, the density of the negative ion $O_2^-$ to be small and the density of the negative ion $O_3^-$ to be negligible in the pressure range of interest, 1–100 mTorr. Dissociative attachment of the oxygen molecule in the ground-state $O_2(^3\Sigma_g^-)$ and the metastable oxygen molecule $O_2(a^1\Delta_g)$ are the dominating channels for the creation of the negative oxygen ion $O^-$. At low pressure (<5 mTorr) recombination involving $O^-$ and $O^+$ ions is the main loss channel for $O^-$ ions. At higher pressure, the detachment on $O(^3P)$ becomes the main loss channel for the $O^-$ ion. The creation of $O_2^-$ is mainly through dissociative attachment of ozone $O_3$. Ozone is almost entirely created through detachment by the collision of $O^-$ with the metastable oxygen molecule $O_2(a^1\Delta_g)$. The creation of $O_2^-$ is thus greatly influenced by this detachment process and neglecting the detachment has a significant influence on the density of $O_2^-$ ions. At low pressure (<10 mTorr) the $O_2^-$ ion is mainly lost through recombination while at higher pressure the charge transfer to form $O_2$ is the dominating loss process.

## 1. Introduction

Oxygen discharges have been applied in plasma processing for decades with applications such as ashing of photoresist [1], removing polymer films and oxidation or deposition of thin-film oxides [2, 3]. Early on, oxygen discharges were successfully produced in capacitive radio frequency (rf) discharges [1, 4]. More recently, low-pressure high-density discharges have been developed and oxygen plasma has been produced in electron cyclotron discharges [2, 5], inductively coupled discharges [6–8] and helicon wave discharges [9, 10]. Oxygen is a simple diatomic gas that has been particularly well studied. However, even in a relatively simple oxygen discharge a number of species can be formed. Fortunately there exists a data set for oxygen including rate coefficients for many of the relevant reactions [11–13], but many of the cross sections for binary processes among these species have not been carefully measured or calculated [13]. Oxygen discharges are weakly electronegative and the negative ions ($O^-$, $O_2^-$, $O_3^-$) are expected to contribute significantly to the overall charge balance in oxygen plasma. The presence of negative ions alters the overall discharge phenomena with additional volume recombination loss and a particular spatial distribution of the negative ions which affects the ion flux loss to the wall [14, 15]. Stoffels *et al* [16] investigated the ion concentration of an oxygen discharge in a conventional parallel plate reactor by microwave resonance combined with laser-induced photodetachment. They found $O^-$ to be the dominant negative ion; however, a significant fraction (∼10%) of $O_2^-$ and $O_3^-$ ions was present in the plasma. Furthermore, Amemiya *et al* [4] estimate the density of $O_2^-$ ions to be comparable to that of $O^-$ ions and the density of $O_3^-$ ions to be negligible at pressures below 150 mTorr in a parallel plate reactor. The metastable molecule $O_2(a^1\Delta_g)$ is suggested to play significant role in capacitive rf discharges in the pressure range 0.005–0.1 Torr [16–19]. Detachment by collisions of ions with the metastable molecule $O_2(a^1\Delta_g)$ and oxygen atoms $O(^3P)$ is suggested to be a significant loss process for the

[3] Present address: Cypress Semiconductor, 3901 North First Street, San Jose, CA 95134, USA.
[4] Present address: PDF Solutions, 333 West San Carlos Street, Suite 700, San Jose, CA 95110, USA.

 © 2001 IOP Publishing Ltd Printed in the UK 

negative oxygen ions [19–21].

The volume averaged global model for high-density discharges was developed by Lieberman and Gottscho [22] for noble gases and extended to molecular gases by Lee *et al* [23, 24]. A more elaborate volume averaged global model of $O_2$ and $Ar/O_2$ mixture has been developed and compared to Langmuir probe and mass spectrometer measurements [25, 26]. The main idea of a global model is to neglect the complexity which arises when spatial variations are considered and to generate a model that encompasses a large number of reactions in order to model a processing plasma with a limited computing power. Thus, the model does not describe spatial distribution but captures scalings of plasma parameters with control parameters. We apply a global (volume averaged) model, described elsewhere [27], to investigate the role of negative ions and metastable atoms and molecules in a high-density oxygen discharge. For this investigation, the number of species and reactions is increased significantly. Furthermore, the formulation for the normalized axial edge densities is revised to account for electronegative discharge and multiple positive ion species. The model allows us to investigate various phenomena, such as the effects of excited species, negative ions and particular reactions on the overall discharge. In an earlier publication [28] we investigated the effect of detachment on the low-pressure oxygen discharge. In this work we investigate which reactions are significant in the creation and destruction of negative ions in a low-pressure oxygen discharge. It should be emphasized that the global model is not meant to apply at high pressures where the assumption of uniform Maxwellian electron energy distribution breaks down. It is most commonly used for low-pressure high-density discharges, in the range 1–20 mTorr for typical powers and discharge dimensions.

## 2. The global (volume averaged) model

We assume a cylindrical chamber of radius $R$ and length $L$. A steady flow $q$ of neutral species is introduced through the inlet. The content of the chamber is assumed to be nearly spatially uniform and the power is deposited uniformly into the plasma bulk. We assume eleven species in the oxygen discharge, electrons, molecular oxygen in ground-state $O_2(^3\Sigma_g^-)$, metastable molecular oxygen $O_2(a^1\Delta_g)$, atomic oxygen in ground-state $O(^3P)$, metastable atomic oxygen $O(^1D)$, ozone $O_3$, the positive ions $O^+$ and $O_2^+$ and the negative ions $O^-$, $O_2^-$ and $O_3^-$. Electrons are assumed to have a Maxwellian energy distribution in the range 1–7 eV. The reactions and rate coefficients assumed in the model are listed in table 1. The plasma chemistry is described by a set of first-order differential equations [23, 27]. For each species a continuity equation describes the creation and the volumetric and surface reactions and losses. For the present study the system of first-order differential equations is allowed to reach a steady state. In addition, the charged particle species must satisfy the quasi-neutrality condition given by

$$n_{O_2^+} + n_{O^+} = n_e + n_{O^-} + n_{O_2^-} + n_{O_3^-} \tag{1}$$

where $n_{O_2^+}$ is the density of $O_2^+$ ions, $n_{O^+}$ is the density of $O^+$ ions, $n_e$ is the density of electrons, $n_{O^-}$ is the density of the negative ion $O^-$, $n_{O_2^-}$ is the density of the negative ion $O_2^-$ and $n_{O_3^-}$ is the density of the negative ion $O_3^-$.

The power balance equation, which equates the absorbed power $P_{abs}$ to power losses due to elastic and inelastic collisions and losses due to charged particle flow to walls, is given as

$$\begin{aligned}\frac{P_{abs}}{V} = &- e\mathcal{E}_c^{(O_2)} k_1 n_{O_2} n_e - k_{51} e\,(\mathcal{E}_e + \mathcal{E}_i)\, n_{O_2^+} \\ &- e\mathcal{E}_c^{(O)} k_4 n_O n_e - k_{50} e\,(\mathcal{E}_e + \mathcal{E}_i)\, n_{O^+}\end{aligned} \tag{2}$$

where $\mathcal{E}_c^{(X)}$ is the energy loss per electron–ion pair created for the neutral X, defined as [22]

$$\mathcal{E}_c = \mathcal{E}_{iz} + \sum_i \mathcal{E}_{ex,i}\frac{k_{ex,i}}{k_{iz}} + \frac{k_{el}}{k_{iz}}\frac{3m_e}{m_i}T_e \tag{3}$$

where $\mathcal{E}_{iz}$ is the ionization energy, $\mathcal{E}_{ex,i}$ is the energy for the $i$th excitation process, $k_{iz}$ is the ionization rate constant, $k_{ex,i}$ is the rate constant for the $i$th excited state and $k_{el}$ is the elastic scattering rate constant. The collisional loss $\mathcal{E}_c^{(O_2^+)}$ is the energy lost per electron–$O_2^+$ ion pair created. $\mathcal{E}_c^{(O^+)}$ is the energy loss per electron–$O^+$ ion pair created. The collisional loss is calculated using the excitation rate constants for atomic and molecular oxygen that were calculated by integrating the excitation cross sections over an assumed Maxwellian electron energy distribution and fitted over an electron temperature range of 1–7 eV, and are listed elsewhere [26]. The estimated uncertainty of the excitation cross-section data is about 25–50%. The plasma potential $V_{pl}$ is calculated self-consistently by equating the flux of positive species to that of negative species [25, 26]. A detailed description of the numerical procedure is given elsewhere [27].

For neutral species, the main sources of $O_2$ are the recombination of oxygen atoms on the chamber walls and the flow of $O_2$ molecules into the reactor, while for the creation of O atoms the dissociation of $O_2$ dominates. The oxygen atoms are mainly lost by recombination of O atoms at the chamber walls. Negative ions are trapped within the discharge by the positive potential of the plasma with respect to all wall surfaces and are assumed to be lost only by recombination with positive ions and detachment in the volume. Negatively charged oxygen ions, $O^-$, play an important role in oxygen discharges. In oxygen plasmas at low gas pressures (<100 mTorr) the $O^-$ ions are mainly produced by dissociative attachment from the ground-state molecule $O_2(X^3\Sigma_g^+)$ and the metastable oxygen molecule $O_2(a^1\Delta_g)$. The cross section for the dissociative electron attachment from the ground-state oxygen molecule $O_2(X^3\Sigma_g^+)$ has a threshold energy of 4.7 eV and a peak value at 6.7 eV [29]. For the lowest electronically excited metastable state of the oxygen molecule $O_2(a^1\Delta_g)$ the threshold is shifted to lower energy by 0.98 eV which is equal to the potential energy difference between the two molecules and the peak value of the cross section is a factor of 3.5 larger for the metastable state [30].

The diffusional losses of atomic oxygen $O(^3P)$, the metastable oxygen atoms $O(^1D)$ and metastable oxygen molecules $O_2(a^1\Delta_g)$ to the reactor walls are estimated by an effective loss-rate coefficient. The effective loss-rate coefficient for atomic oxygen is given by [31]

$$k_{dl} = \left[\frac{\Lambda_O^2}{D_O} + \frac{2V\,(2-\gamma_O)}{A v_O \gamma_O}\right]^{-1} \tag{4}$$

**Table 1.** The reaction set for oxygen. The rate coefficients for electron impact collisions were calculated assuming Maxwellian electron energy distribution and fitted over an electron temperature range 1–7 eV.

| Reaction | Rate coefficient | Reference |
|---|---|---|
| $e + O_2 \longrightarrow O_2^+ + 2e$ | $k_1 = 9 \times 10^{-16} T_e^2 \exp(-12.6/T_e)$ m$^3$ s$^{-1}$ | [23] |
| $e + O_2^+ \longrightarrow O(^3P) + O(^3P)$ | $k_2 = 2.2 \times 10^{-13}$ m$^3$ s$^{-1}$ | [11] |
| $e + O_2 \longrightarrow O(^3P) + O^-$ | $k_3 = 8.8 \times 10^{-17} \exp(-4.4/T_e)$ m$^3$ s$^{-1}$ | [46] |
| $e + O(^3P) \longrightarrow O^+ + 2e$ | $k_4 = 9.0 \times 10^{-15} T_e^{0.7} \exp(-13.6/T_e)$ m$^3$ s$^{-1}$ | [46] |
| $O^- + O_2^+ \longrightarrow O(^3P) + O_2$ | $k_5 = 1.5 \times 10^{-13} (300/T_g)^{1/2}$ m$^3$ s$^{-1}$ | [23] |
| $O^- + O^+ \longrightarrow O(^3P) + O(^3P)$ | $k_6 = 2.7 \times 10^{-13} (300/T_g)^{1/2}$ m$^3$ s$^{-1}$ | [11] |
| $e + O^- \longrightarrow O(^3P) + 2e$ | $k_7 = 1.1 \times 10^{-13} \exp(-3.58/T_e)$ m$^3$ s$^{-1}$ | [47] |
| $e + O_2 \longrightarrow O(^3P) + O(^3P) + e$ | $k_8 = 7.1 \times 10^{-15} \exp(-8.6/T_e)$ m$^3$ s$^{-1}$ | [11] |
| $O(^3P) + O^- \longrightarrow O_2 + e$ | $k_9 = 3.0 \times 10^{-16} (300/T_g)^{1/2}$ m$^3$ s$^{-1}$ | [46] |
| $e + O_2 \longrightarrow O^- + O^+ + e$ | $k_{10} = 7.1 \times 10^{-17} T_e^{0.5} \exp(-17/T_e)$ m$^3$ s$^{-1}$ | [46] |
| $e + O_2 \longrightarrow O(^3P) + O^+ + 2e$ | $k_{11} = 5.3 \times 10^{-16} T_e^{0.9} \exp(-20/T_e)$ m$^3$ s$^{-1}$ | [46] |
| $O^+ + O_2 \longrightarrow O(^3P) + O_2^+$ | $k_{12} = 2 \times 10^{-17} (300/T_g)^{1/2}$ m$^3$ s$^{-1}$ | [11] |
| $e + O_2 \longrightarrow O(^3P) + O(^1D) + e$ | $k_{13} = 1.8 \times 10^{-13} \exp(-18.33/T_e)$ m$^3$ s$^{-1}$ | [11] |
| $e + O(^3P) \longrightarrow O(^1D) + e$ | $k_{14} = 4.5 \times 10^{-15} \exp(-2.29/T_e)$ m$^3$ s$^{-1}$ | [23] |
| $O(^1D) + O_2 \longrightarrow O(^3P) + O_2$ | $k_{15} = 3.0 \times 10^{-17}$ m$^3$ s$^{-1}$ | [11] |
| $O(^1D) + O(^3P) \longrightarrow 2O(^3P)$ | $k_{16} = 8.1 \times 10^{-18}$ m$^3$ s$^{-1}$ | [23] |
| $e + O(^1D) \longrightarrow O^+ + 2e$ | $k_{17} = 9 \times 10^{-15} T_e^{0.7} \exp(-11.6/T_e)$ m$^3$ s$^{-1}$ | [23] |
| $e + O_2 \longrightarrow O_2(a^1\Delta_g) + e$ | $k_{18} = 1.7 \times 10^{-15} \exp(-3.1/T_e)$ m$^3$ s$^{-1}$ | [46] |
| $e + O_2(a^1\Delta_g) \longrightarrow O_2^+ + 2e$ | $k_{19} = 9.0 \times 10^{-16} T_e^2 \exp(-11.6/T_e)$ m$^3$ s$^{-1}$ | [46] |
| $e + O_2(a^1\Delta_g) \longrightarrow O^- + O$ | $k_{20} = 2.28 \times 10^{-16} \exp(-2.29/T_e)$ m$^3$ s$^{-1}$ | [30] |
| $e + O_2(a^1\Delta_g) \longrightarrow O_2 + e$ | $k_{21} = 5.6 \times 10^{-15} \exp(-2.2/T_e)$ m$^3$ s$^{-1}$ | [46] |
| $e + O_2(a^1\Delta_g) \longrightarrow 2O + e$ | $k_{22} = 4.2 \times 10^{-15} \exp(-4.6/T_e)$ m$^3$ s$^{-1}$ | [46] |
| $O^- + O_2(a^1\Delta_g) \longrightarrow O_2^- + O(^3P)$ | $k_{23} = 1.1 \times 10^{-17} (300/T_g)^{1/2}$ m$^3$ s$^{-1}$ | [41] |
| $O_2^- + O_2^+ \longrightarrow O_2$ | $k_{24} = 2.0 \times 10^{-13} (300/T_g)^{1/2}$ m$^3$ s$^{-1}$ | [46] |
| $O_2^- + O^+ \longrightarrow O_2 + O(^3P)$ | $k_{25} = 2.0 \times 10^{-13} (300/T_g)^{1/2}$ m$^3$ s$^{-1}$ | [46] |
| $e + O_2 + O_2 \longrightarrow O_2^- + O_2$ | $k_{26} = 2.26 \times 10^{-42} (300/T_g)^{1/2}$ m$^3$ s$^{-1}$ | [48] |
| $O^- + O^+ \longrightarrow O(^3P) + O(^1D)$ | $k_{27} = 4.9 \times 10^{-16} (300/T_g)^{1/2}$ m$^3$ s$^{-1}$ | [43] |
| $O_2^- + O_2(a^1\Delta_g) \longrightarrow 2O_2 + e$ | $k_{28} = 2.7 \times 10^{-17} (300/T_g)^{1/2}$ m$^3$ s$^{-1}$ | [41] |
| $O_2^- + O(^3P) \longrightarrow O^- + O_2$ | $k_{29} = 3.31 \times 10^{-16} (300/T_g)^{1/2}$ m$^3$ s$^{-1}$ | [11] |
| $e + O_3 \longrightarrow O^- + O_2$ | $k_{30} = 9.3 \times 10^{-16}/T_e^{0.62}$ m$^3$ s$^{-1}$ | [45] |
| $e + O_3 \longrightarrow O + O_2^-$ | $k_{31} = 2.0 \times 10^{-16}$ m$^3$ s$^{-1}$ | [45] |
| $O^- + O_2 \longrightarrow O_3 + e$ | $k_{32} = 5.0 \times 10^{-21} (300/T_g)^{1/2}$ m$^3$ s$^{-1}$ | [12] |
| $O^- + O_2(a^1\Delta_g) \longrightarrow O_3 + e$ | $k_{33} = 2.2 \times 10^{-17} (300/T_g)^{1/2}$ m$^3$ s$^{-1}$ | [41] |
| $O^+ + O_3 \longrightarrow O_2^+ + O_2$ | $k_{34} = 1.0 \times 10^{-17} (300/T_g)^{1/2}$ m$^3$ s$^{-1}$ | [46] |
| $O + O_3 \longrightarrow 2O_2$ | $k_{35} = 2.0 \times 10^{-17} (300/T_g)^{1/2}$ m$^3$ s$^{-1}$ | [46] |
| $O^- + O_3 \longrightarrow O_3^- + O$ | $k_{36} = 5.3 \times 10^{-16} (300/T_g)^{1/2}$ m$^3$ s$^{-1}$ | [11] |
| $O_3^- + O(^3P) \longrightarrow O_2^- + O_2$ | $k_{37} = 3.2 \times 10^{-16} (300/T_g)^{1/2}$ m$^3$ s$^{-1}$ | [12] |
| $O_3^- + O(^3P) \longrightarrow 2O_2 + e$ | $k_{38} = 3.0 \times 10^{-16} (300/T_g)^{1/2}$ m$^3$ s$^{-1}$ | [12] |
| $O_3^- + O_2^+ \longrightarrow O_2 + O_3$ | $k_{39} = 2 \times 10^{-13} (300/T_g)^{1/2}$ m$^3$ s$^{-1}$ | [11] |
| $O_3^- + O_2^+ \longrightarrow 2O + O_3$ | $k_{40} = 1.01 \times 10^{-13} (300/T_g)^{1/2}$ m$^3$ s$^{-1}$ | [11] |
| $O_2^- + O_3 \longrightarrow O_2 + O_3^-$ | $k_{41} = 4 \times 10^{-16} (300/T_g)^{1/2}$ m$^3$ s$^{-1}$ | [11] |
| $O_2^- + O(^3P) \longrightarrow O_3 + e$ | $k_{42} = 3.01 \times 10^{-16} (300/T_g)^{1/2}$ m$^3$ s$^{-1}$ | [11] |
| $e + O_3 \longrightarrow O(^3P) + O_2 + e$ | $k_{43} = 1 \times 10^{-14} (300/T_g)^{1/2}$ m$^3$ s$^{-1}$ | [11] |
| $2O_2 + O(^3P) \longrightarrow O_3 + O_2$ | $k_{44} = 6.9 \times 10^{-40} (300/T_g)^{-1.25}$ [$O_2$] m$^3$ s$^{-1}$ | [11] |
| $O_2^- + 2O(^3P) \longrightarrow O_3 + O(^3P)$ | $k_{45} = 3.82 \times 10^{-40}$ [O] m$^3$ s$^{-1}$ | [11] |
| $e + O(^3P) + O_2 \longrightarrow O_2^- + O(^3P)$ | $k_{46} = 1 \times 10^{-43}$ m$^6$ s$^{-1}$ | [11] |
| $e + O(^3P) + O_2 \longrightarrow O^- + O_2$ | $k_{47} = 1 \times 10^{-43}$ m$^6$ s$^{-1}$ | [11] |
| $e + O_2^+ \longrightarrow O(^1D) + O(^3P)$ | $k_{48} = 2.11 \times 10^{-13} (300/T_g)^{0.7}$ m$^3$ s$^{-1}$ | [11] |
| $O_2^+ + O(^1D) \longrightarrow O_2(a^1\Delta_g) + O(^3P)$ | $k_{49} = 1.0 \times 10^{-18} (300/T_g)^{0.5}$ m$^3$ s$^{-1}$ | [11] |
| $T_g$ (K)<br>$T_e$ (eV) | | |

**Table 2.** The interaction of atomic and molecular oxygen with the reactor walls.

| Reaction | $\gamma$ | Rate coefficient |
|---|---|---|
| $O^+(g) \longrightarrow O(^3P)(g)$ | | $k_{50} = 2u_{B,O^+}(R^2h_L + RLh_R)/R^2L\ s^{-1}$ |
| $O_2^+(g) \longrightarrow O_2(g)$ | | $k_{51} = 2u_{B,O_2^+}(R^2h_L + RLh_R)/R^2L\ s^{-1}$ |
| $O(^3P)(g) \longrightarrow \frac{1}{2}O_2(g)$ | $\gamma_O = 0.17$ [35] | $k_{52} = \left[\frac{\Lambda_0^2}{D_O} + \frac{2V(2-\gamma_O)}{Av_O\gamma_O}\right]^{-1}\ s^{-1}$ |
| $O(^1D)(g) \longrightarrow \frac{1}{2}O_2(g)$ | $\gamma_{O^*} = 0.17$ [35] | $k_{53} = \left[\frac{\Lambda_0^2}{D_{O^*}} + \frac{2V(2-\gamma_{O^*})}{Av_{O^*}\gamma_{O^*}}\right]^{-1}\ s^{-1}$ |
| $O_2^M(g) \longrightarrow O_2(g)$ | $\gamma_{O_2^M} = 0.007$ [37] | $k_{54} = \left[\frac{\Lambda_0^2}{D_{O_2^*}} + \frac{2V(2-\gamma_{O_2^*})}{Av_{O_2^M}\gamma_{O_2^M}}\right]^{-1}\ s^{-1}$ |

where $D_O$ is the neutral diffusion coefficient given by

$$D_O = \frac{eT_g\lambda_i}{v_O m_O}. \tag{5}$$

$v_O = (8eT_g/\pi m_O)^{1/2}$ is the mean neutral speed, $\gamma_O$ is the sticking coefficient for atomic oxygen on the wall surface, $V$ and $A$ are the volume and the wall surface area of the reactor chamber, respectively, and $\lambda_i$ is the mean free path. The effective diffusion length of each of the neutral species is given by [32]

$$\Lambda_O = \left[\left(\frac{\pi}{L}\right)^2 + \left(\frac{2.405}{R}\right)^2\right]^{-1/2}. \tag{6}$$

The effective loss-rate coefficients for neutrals and positive ions are listed in table 2.

### 2.1. Effective surface area

The effective area of a cylindrical discharge is defined as [22]

$$A_{eff} = 2\pi R\,(Rh_L + Lh_R) \tag{7}$$

where $h_L$ and $h_R$ are the axial and radial sheath edge densities, respectively, normalized to the bulk density. In weakly electronegative discharges, the plasma is generally divided into two regions: an electronegative core and an electropositive edge [14]. Furthermore, there is a sheath between the plasma and an external wall. The electronegative core consists primarily of positive and negative ions, with a smaller component of electrons. In the electropositive edge, negative ion density is negligible. At the sheath edge, the positive ions reach the Bohm velocity and the concentration is $n_{s+}$. The ratio of the positive ion sheath edge density $n_{s+}$ to the electron density at the axial boundary with the electronegative region $n_{e0}$ is given by [33]

$$h_L = \frac{n_{s+}}{n_{e0}} = \left(\frac{1+\chi_0^{3/2}}{1+\chi_s^{3/2}}\right)^{1/3} \tag{8}$$

where $\chi$ is a non-dimensional electric field and the subscripts 0 and s refer to the electronegative region boundary and the sheath boundary, respectively. The non-dimensional electric field at the sheath edge is

$$\chi_s = \beta^{-2/3}\left(\sum_j c_j \frac{\pi(\ell_p - \ell_-)}{2\lambda_{i,j}}\right)\left(\sum_j c_j\right)^{-1} \tag{9}$$

where the electropositive region extends from $\ell_-$, the edge of the electronegative region, to $\ell_p > \ell_-$ the plasma sheath edge. Here

$$c_j = \nu_{iz,j}\left(\frac{\pi m_{i,j}}{2e\lambda_{i,j}}\right)^{1/2} \tag{10}$$

and

$$\beta = \sum_j \left(\frac{\pi(\ell_p - \ell_-)}{2\lambda_{i,j}}\right)^{1/2} \frac{\nu_{iz,j}(\ell_p - \ell_-)}{u_{B0,j}} \tag{11}$$

where $u_{B0,j} = (eT_e/m_{i,j})^{1/2}$ is the Bohm velocity, $\nu_{iz,j} = n_{g,j}k_{iz,j}$ is the ionization rate, $n_{g,j}$ is the neutral density, $k_{iz,j}$ is the rate coefficient for the ionization reaction which produces the $j$th ion and $\lambda_{i,j}$ is the ion-neutral mean free path

$$\lambda_{i,j} = \frac{1}{n_{g,j}\sigma_{i,j}} \tag{12}$$

where $n_{g,j}$ refers to neutral species of the $j$th ion and $\sigma_{i,j}$ is the ion-neutral scattering cross section for the $j$th neutral. The total ionic momentum transfer cross section for atomic oxygen is $\sigma_i = 7.5 \times 10^{-19}$ m$^2$ [34]. We assume the ionic momentum transfer cross section for molecular oxygen to be $\sigma_i = 7.5 \times 10^{-19}$ m$^2$ as well.

The electric field at the electronegative region boundary is obtained as

$$\chi_0 = \beta^{-2/3}\frac{\pi(\ell_p - \ell_-)}{2\lambda_{i,j}}w_j^2 \tag{13}$$

where $w_j = u_{in,j}/u_{B,j}$, $u_{in,j}$ is the velocity of the $j$th positive ion entering the electropositive region and $u_{B,j}$ is the Bohm velocity of the positive ion $j$. As long as the diffusion flux is negligible in comparison to the mobility flux, $w_j^2/\lambda_{i,j}$, is the same for all positive species and we can use any $w_j$ in equation (13). This is due to the fact that the ion drift velocity is determined by the electric field alone. However, inside the negative core there is a diffusion flux contribution that is of same order as the mobility contribution in the electropositive edge.

As an approximation we find a density averaged value for $w_j^2/\lambda_{i,j}$

$$\overline{\left(w_j^2/\lambda_{i,j}\right)} = \frac{\sum_{l=0}^{N_+} n_{+,l}\left(u_{in,l}/u_{B,l}\right)^2/\lambda_{i,l}}{\sum_{l=0}^{N_+} n_{+,l}} \tag{14}$$

where $N_+$ is the total number of positive ion species considered in the discharge. Assuming that, for a weakly electronegative discharge, drift-diffusion dominates the positive–negative ion

**Table 3.** The diffusion coefficients for positive oxygen ions and neutrals in a stainless steel cylindrical discharge with radius $R = 15.2$ cm, length $L = 7.6$ cm, an applied power of 500 W, a flow rate $q = 50$ sccm and a neutral gas temperature of $T_g = 600$ K.

| | 1 mTorr | 10 mTorr |
|---|---|---|
| $D_{O^+}$ $(m^2\ s^{-1})$ | 14.7 | 2.1 |
| $D_{O_2^+}$ $(m^2\ s^{-1})$ | 10.0 | 1.4 |
| $D_O$ $(m^2\ s^{-1})$ | 8.8 | 1.2 |
| $D_{O_2}$ $(m^2\ s^{-1})$ | 6.3 | 0.84 |

recombination flux in the electronegative core, the positive ions enter the electropositive region at velocity

$$u_{\mathrm{in},j} = \frac{2\bar{D}_{\mathrm{a},j}\alpha_0}{L} \tag{15}$$

where $\bar{\alpha} = \sum_{i=1}^{N_-} n_{-,i}/n_e$, $\alpha_0 = \frac{3}{2}\bar{\alpha} = n_{-0}/n_{e0}$ and $D_{a,j}$ is the ambipolar diffusion coefficient for species $j$ in an arbitrary mixture of charged particles. For the volume averaged discharge

$$\bar{D}_{\mathrm{a},j} \approx D_j \frac{1+\gamma+2\gamma\bar{\alpha}}{1+\gamma\bar{\alpha}} \tag{16}$$

where $\gamma = T_e/T_j$, $D_j = eT_j/(m_j\nu_j) = v_{T_j}\lambda_{i,j}$ where $\nu_j$ is the total momentum transfer collision frequency, $T_j$ is the species temperature in volts and $v_{T_j} = (eT_j/m_j)^{1/2}$. Unfortunately, no solution exists for the normalized radial sheath edge density of a weakly electronegative plasma so we assume $h_R = h_L$ in this study. This is reasonable for a short cylindrical discharge, $L < 2R$, which we treat below.

### *2.2. Wall sticking coefficient*

The densities of the atomic oxygen and metastable oxygen molecule are largely determined by their interactions with the wall. Using a global (volume averaged) model Lee and Lieberman [24] showed that the fractional dissociation, and thus the ionic composition in oxygen discharges, depend strongly on the wall recombination coefficient. Booth and Sadeghi [31] estimate the wall sticking coefficient for atomic oxygen in pure oxygen plasma on stainless steel wall to be $\gamma_O \approx 0.5$. Similarly Granier *et al* [10] propose $\gamma_O$ to be in the range $0.1 < \gamma_O < 1$ for stainless steel. In this work we use the measured recombination coefficient of O radicals on stainless steel walls of $\gamma_O = 0.17 \pm 0.02$ at 300 K from Singh *et al* [35]. However, we should note that a significant portion of the surface area of an inductive discharge is a quartz window. Greaves and Linnett [36] give a recombination coefficient of $1.8 \times 10^{-4}$ for quartz at 300 K. The effective recombination coefficient in a typical inductive discharge is thus somewhat lower than the 0.17 assumed here.

The importance of the metastable oxygen molecule $O_2(a^1\Delta_g)$ is known to depend heavily on the surface sticking coefficient [17]. Sharpless and Slanger [37] measured the quenching of $O_2(a^1\Delta_g)$ on metal surfaces and report a value $\gamma_{O_2^M} = 0.007$ for an Fe surface and $\gamma_{O_2^M} \leqslant 10^{-3}$ for an aluminium surface. We assume the surface sticking coefficient for ozone $O_3$ to be zero.

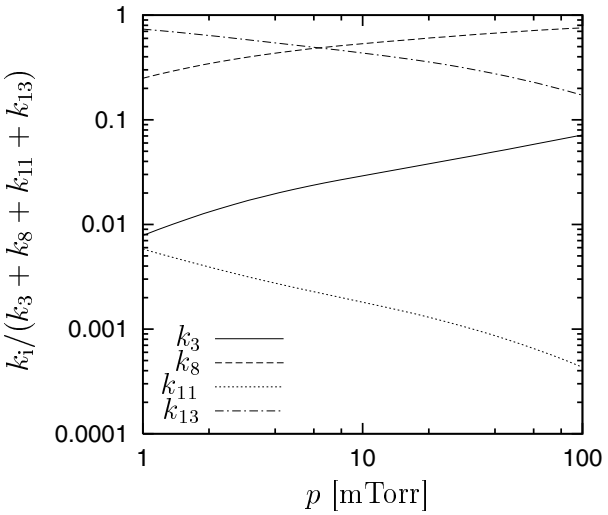


**Figure 1.** Relative contribution of various dissociation channels for electron impact dissociation of molecular oxygen in the ground-state $O_2(^3\Sigma_g^-)$ to form oxygen atom in the ground-state $O(^3P)$, dissociative attachment $k_3$ ($e + O_2 \longrightarrow O(^3P) + O^-$), dissociation $k_8$ ($e + O_2 \longrightarrow 2O(^3P) + e$) and $k_{13}$ ($e + O_2 \longrightarrow O(^3P) + O(^1D) + e$) and dissociative ionization $k_{11}$ ($e + O_2 \longrightarrow O(^3P) + O^+ 2e$), versus the discharge pressure at 500 W and a flow rate of 50 sccm. We assume a cylindrical stainless steel chamber with $L = 7.6$ cm and $R = 15.2$ cm.

## 3. Discussion

We apply the global (volume averaged) model to a cylindrical discharge in a stainless steel chamber with radius $R = 15.2$ cm and length $L = 7.6$ cm. We assume an applied power of 500 W, a flow rate $q = 50$ sccm and a neutral gas temperature of $T_g = 600$ K. Since the densities of the atomic oxygen and the metastable oxygen molecule are largely determined by their interactions with the wall, the chamber material and geometry have a decisive influence on the properties of the discharge. The calculated diffusion coefficents for positive ions and neutrals used in the model are listed in table 3 for discharge operated at 1 mTorr and 10 mTorr.

Atomic oxygen is produced mainly by dissociative excitation of oxygen molecules by electron impact and by dissociative attachment. In figure 1 we compare the relative contributions of various dissociation channels for electron impact dissociation of molecular oxygen in the ground-state $O_2(^3\Sigma_g^-)$ to form oxygen atoms in the ground-state $O(^3P)$. We compare the ratio of the rate constants for dissociative attachment $k_3$ ($e + O_2 \longrightarrow O(^3P) + O^-$), dissociation $k_8$ ($e + O_2 \longrightarrow 2O(^3P) + e$) and $k_{13}$ ($e + O_2 \longrightarrow O(^3P) + O(^1D) + e$) and dissociative ionization $k_{11}$ ($e + O_2 \longrightarrow O(^3P) + O^+ + 2e$). Figure 1 shows the ratio of $k_3$, $k_8$, $k_{11}$ and $k_{13}$ to the sum $(k_3 + k_8 + k_{11} + k_{13})$ versus the discharge pressure. We see that the majority of dissociation (>99%) occurs through the 8.4 and 6.0 eV excited states (reactions 8 and 13). We note that reaction 13 is the dominating dissociation channel for discharge pressure below 5 mTorr but reaction 8 is the dominating dissociation channel for higher pressure. Thus, lower pressure favours the creation of the metastable oxygen atom $O(^1D)$. The rates of dissociative attachment (reaction 3) and dissociative ionization (reaction 11) are

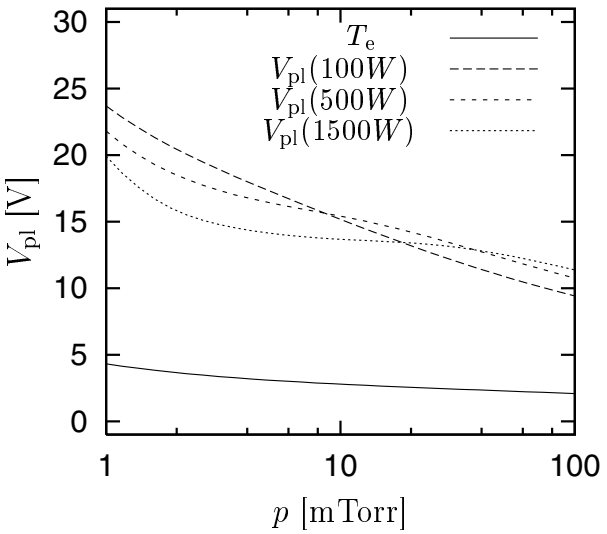


**Figure 2.** The electron temperature $T_e$ and the plasma potential $V_{pl}$ versus discharge pressure at 100, 500 and 1500 W. We assume a flow rate of 50 sccm and a cylindrical stainless steel chamber with $L = 7.6$ cm and $R = 15.2$ cm.

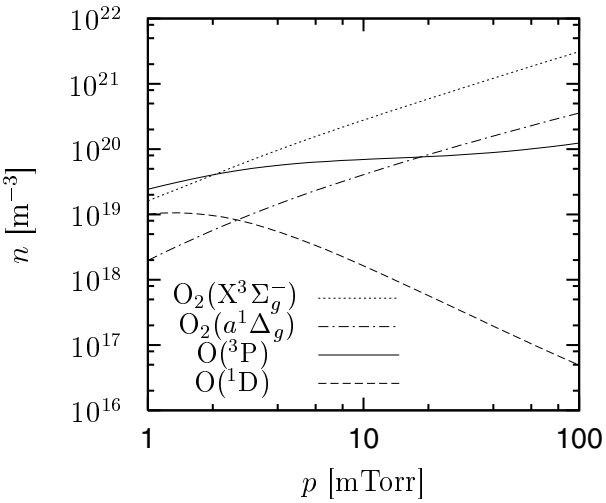


**Figure 3.** The neutral densities of atomic and molecular oxygen as well as the lowest excited states versus discharge pressure at 500 W and a flow rate of 50 sccm. We assume a cylindrical stainless steel chamber with $L = 7.6$ cm and $R = 15.2$ cm.

found to be insignificant dissociation channels. Another effective channel for the creation of the metastable oxygen atom O($^1$D) is through electron excitation of the ground-state oxygen atom (reaction 14). We find the reaction rate ratio $n_e n_{O_2} k_{13}/(n_e n_O k_{14})$ to be roughly 0.5 in the pressure range of interest. The lowest threshold energy for dissociation of the oxygen molecule is 4.5 eV. However, the lowest lying metastable state of the oxygen molecule $O_2(a^1\Delta_g)$ has a threshold energy of 0.98 eV above the ground state and has a lifetime of $\sim$ 4400 s [38]. The density of the metastable oxygen molecule $O_2(a^1\Delta_g)$ is generally considered to be significant in oxygen discharges and simple calculations show that it is roughly 12 % of the ground-state $O_2(^3\Sigma_g^-)$ density at 10 mTorr and $\gamma_O = 0.5$ [28]. Figure 2 shows the electron temperature and plasma potential versus pressure. The electron temperature decreases with increasing pressure but is roughly independent of applied power. The plasma potential $V_{pl}$, however, depends on the applied power and is shown versus pressure for 100, 500 and 1500 W. The change in the plasma potential $V_{pl}$ with power is due to the change in the mix of ions escaping to the walls and the electronegativity ratio $n_-/n_e$ with power.

Figure 3 shows the density of neutral oxygen atoms in the ground-state O($^3$P) and ground-state oxygen molecules $O_2(^3\Sigma_g^-)$ as well as the lowest excited states of oxygen atoms O($^1$D) and oxygen molecules $O_2(a^1\Delta_g)$. We notice that the density of the metastable oxygen molecule $O_2(a^1\Delta_g)$ is significant. This is consistent with what has commonly been observed for capacitive rf discharges [17,18] and dc discharges [21]. At low pressure, below 2 mTorr, the ground-state oxygen atom O($^3$P) is the dominating neutral. With increasing pressure the ground-state oxygen molecule $O_2(^3\Sigma_g^-)$ becomes the dominating neutral. In the pressure range of interest for low-pressure high-density oxygen discharges (<20 mTorr) there is a significant density of ground-state atomic oxygen in the discharge. The density of the metastable oxygen atom O($^1$D) is significant at low pressure (<3 mTorr) but decreases with increasing pressure and is negligible for pressures above 10 mTorr. The ozone $O_3$ density is negligible compared to the other neutrals in the discharge in the pressure range of interest, roughly $10^{14}$ m$^{-3}$ at 1 mTorr and $10^{17}$ m$^{-3}$ at 100 mTorr.

### *3.1. Comparison with experiments*

In a separate publication [26] we compared global model calculations for an oxygen discharge (assuming fewer species and reactions) to measurements of electron density and effective electron temperature measured by a Langmuir probe and to relative densities of positive ions measured by a mass spectrometer. Fuller *et al* [39] report on measurements of the densities of the ground-state atomic and molecular oxygen and the O($^1$D) and O($^1$S) metastable species of atomic oxygen in an inductively coupled plasma source measured by optical emission actinometry. Here, in figure 4, we compare the densities of ground-state atomic and molecular oxygen and the metastable atomic oxygen O($^1$D) calculated by the global model to their measurements. The cylindrical stainless-steel chamber was 36 cm inside diameter and 22 cm in height. The operating pressure was 10 mTorr and the $O_2$ flow rate was 95 sccm. We see that the global model calculations give fairly good estimates of the neutral densities.

### *3.2. Positive ions*

The densities of the positive ions in oxygen discharge are shown versus discharge pressure in figure 5 for applied powers of 100 and 500 W. Below roughly 8 mTorr, $O^+$ dominates as a positive ion, and above 10 mTorr $O_2^+$ dominates for an applied power of 500 W. At 100 W the $O_2^+$ ion is the dominant positive ion in the pressure range of interest. We note that the density of the $O_2^+$ ion remains relatively independent of power and pressure in the range investigated. For an applied power of 500 W it is $2.8 \times 10^{16}$ m$^{-3}$ at 1 mTorr, $5.7 \times 10^{16}$ m$^{-3}$ at 10 mTorr and $4.5 \times 10^{16}$ m$^{-3}$ at 100 mTorr, and for an applied power of 100 W it is $2.9 \times 10^{16}$ m$^{-3}$ at 10 mTorr and $2.0 \times 10^{16}$ m$^{-3}$ at 100 mTorr.

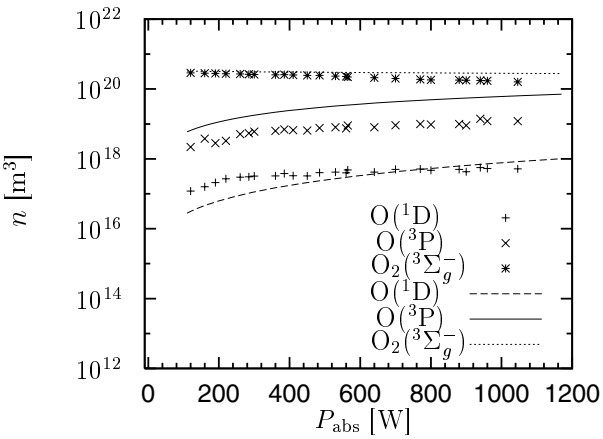


**Figure 4.** The neutral densities of atomic and molecular oxygen as well as the lowest excited states versus absorbed power. The measurements by Fuller *et al* [39] were made in an inductively coupled discharge in a cylindrical stainless steel chamber with $R = 18$ cm and $L = 22$ cm. The operating pressure was 10 mTorr.

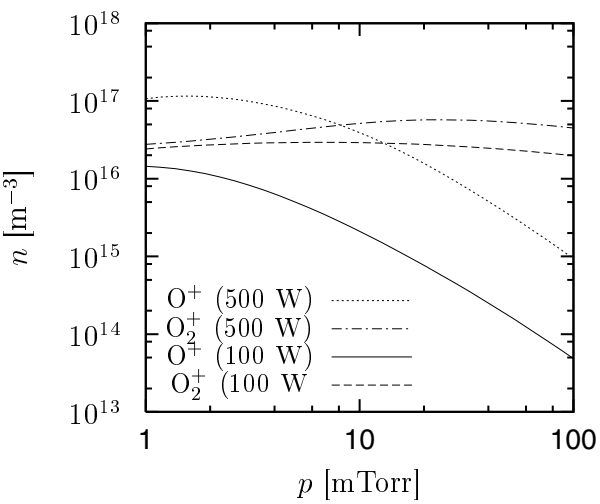


**Figure 5.** The densities of the positive oxygen ions, $O^+$ and $O_2^+$, versus discharge pressure at 500 W and a flow rate of 50 sccm for a cylindrical stainless steel chamber with $L = 7.6$ cm and $R = 15.2$ cm.

### *3.3. Negative ions*

Figure 6 shows the densities of the negative ions versus discharge pressure. The $O^-$ ion is the dominant negative ion in an oxygen discharge, the density of the negative ion $O_2^-$ is small and the density of $O_3^-$ is negligible, in the pressure range of interest.

At 100 mTorr the ratio of the density of the negative oxygen molecule $O_2^-$ to the density of the negative oxygen atom $O^-$ is $[O_2^-]/[O^-] \approx 0.04$, at 10 mTorr $[O_2^-]/[O^-] \approx 0.007$ and at 1 mTorr $[O_2^-]/[O^-] \approx 0.0005$. The importance of $O_2^-$ increases with increasing pressure. Measurements of negative ion densities in a capacitive rf discharge in the pressure range 70–350 mTorr indicate that $O_2^-$ ions are less than 2% of all negative ions [19].

The electronegativity of an oxygen discharge is shown versus pressure in figure 7. The electronegativity $\alpha = n_{O^-}/n_e$, as predicted by the global model, decreases with increased

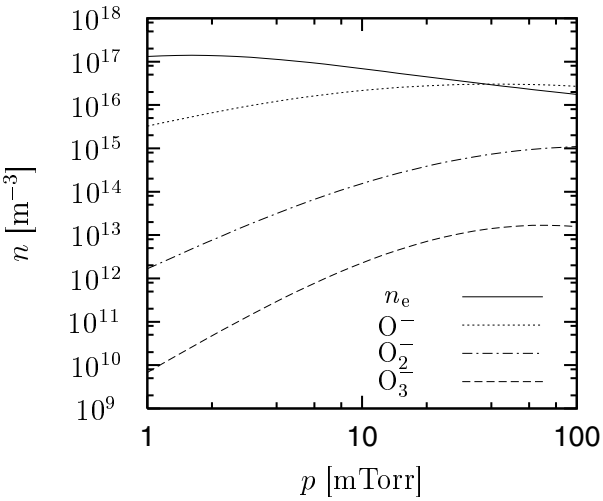


**Figure 6.** The densities of electrons $n_e$ and negative oxygen ions, $O^-$, $O_2^-$, and $O_3^-$, versus discharge pressure at 500 W and a flow rate of 50 sccm for a cylindrical stainless steel chamber with $L = 7.6$ cm and $R = 15.2$ cm.

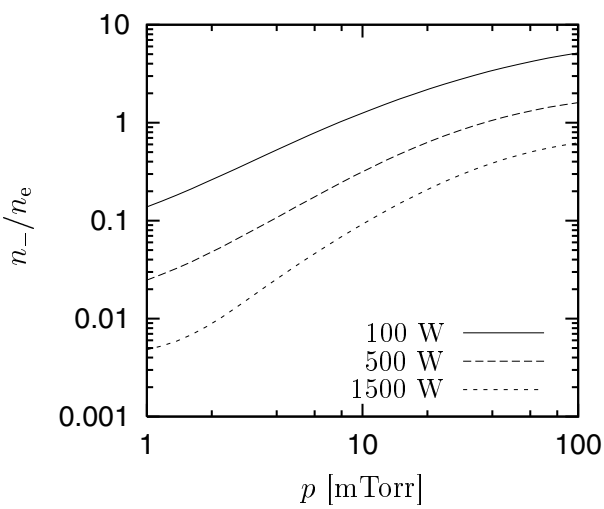


**Figure 7.** The electronegativity $n_e/(n_- + n_{2-} + n_{3-})$ at 100, 500 and 1500 W versus discharge pressure. We assume a flow rate of 50 sccm and a cylindrical stainless steel chamber with $L = 7.6$ cm and $R = 15.2$ cm.

power and increases with increased pressure as shown in figure 7 and is in the range 0.005–5 for the range of powers and pressures studied. This is qualitatively consistent with the measurements by Tuszewski [40], and it is also consistent with the diffusion model that we have assumed, in which the plasma contains both an electronegative core and an electropositive edge [33].

### *3.4. The negative ion $O^-$*

Since the negative ions are trapped within the discharge, creation and destruction of negative ions is through reactions within the volume. In figure 8 we compare the reaction rates $R$ for creation and destruction of the negative oxygen ion $O^-$. In figure 8($a$) the reaction rates for creation of the negative oxygen ion $O^-$ are plotted versus pressure. Dissociative attachment of

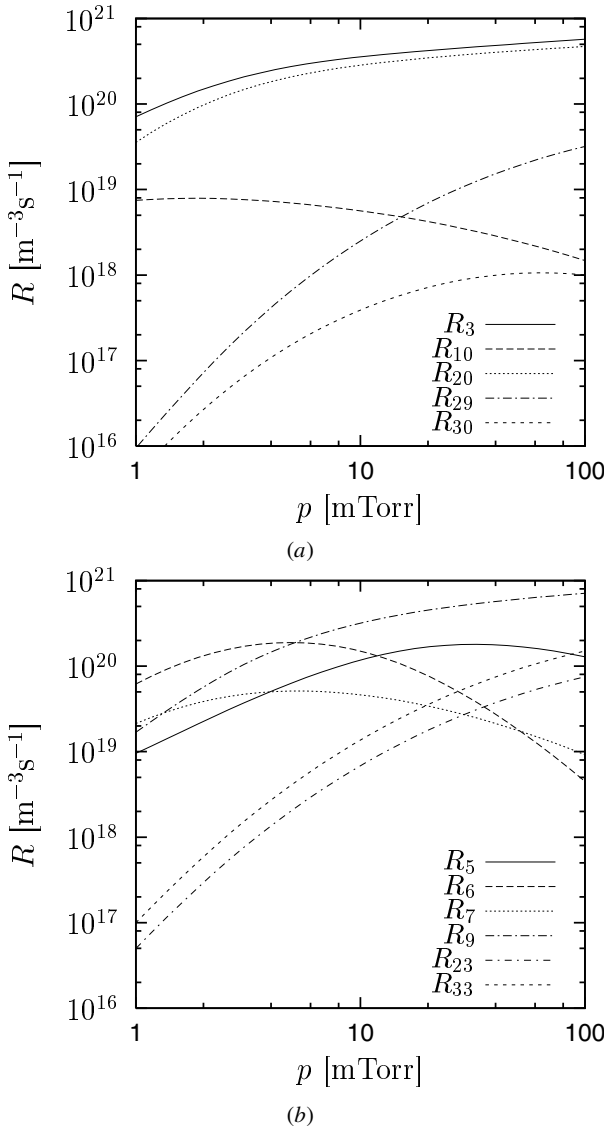


**Figure 8.** The reaction rates $R$ for ($a$) creation of the oxygen ion $O^-$ and ($b$) destruction of the oxygen ion $O^-$ versus discharge pressure at 500 W and a flow rate of 50 sccm for a cylindrical stainless steel chamber with $L = 7.6$ cm and $R = 15.2$ cm.

the oxygen molecule in ground-state $O_2(^3\Sigma_g^-)$

$$e + O_2(^3\Sigma_g^-) \longrightarrow O(^3P) + O^- \qquad \text{(Reaction 3)}$$

with reaction rate $R_3 = k_3 n_e n_{O_2}$ and dissociative attachment of the metastable oxygen molecule $O_2(a^1\Delta_g)$

$$e + O_2(a^1\Delta_g) \longrightarrow O(^3P) + O^- \qquad \text{(Reaction 20)}$$

with reaction rate $R_{20} = k_{20} n_e n_{O_2^M}$ are the dominating channels for the creation of the $O^-$ ion in the pressure range investigated. The rate coefficient for the dissociative attachment of the metastable oxygen molecule $k_{20}$ was calculated from the cross section measured by Burrow [30] and is valid for $1 < T_e < 4.5$ eV. The contributions from other channels, such as polar dissociation (reaction 10) and detachment by $O_2^-$ collisions with $O(^3P)$ (reaction 29), are an order of magnitude smaller.

In figure 8($b$) we show the reaction rates for destruction of the negative ion $O^-$ versus discharge pressure. The main loss mechanism at low pressure (<5 mTorr) is recombination

$$O^- + O^+ \longrightarrow O(^3P) + O(^3P) \qquad \text{(Reaction 6)}$$

with reaction rate $R_6 = k_6 n_{O^-} n_{O^+}$. There is also a significant contribution from detachment by $O^-$ collisions with $O(^3P)$

$$O(^3P) + O^- \longrightarrow e + O_2(^3\Sigma_g^-) \qquad \text{(Reaction 9)}$$

with reaction rate $R_9 = k_9 n_O n_{O^-}$, which becomes the dominating loss mechanism at higher pressure (>5 mTorr). This is consistent with the findings of Ivanov *et al* [21]. Detachment by electron impact from the negative ion $O^-$

$$e + O^- \longrightarrow O(^3P) + 2e \qquad \text{(Reaction 7)}$$

with reaction rate $R_7 = k_7 n_e n_{O^-}$, also contributes to the loss of $O^-$ ions in particular at low pressure. Recombination

$$O^- + O_2^+ \longrightarrow O(^3P) + O_2(^3\Sigma_g^-) \qquad \text{(Reaction 5)}$$

with reaction rate $R_5 = k_5 n_{O_2^+} n_{O^-}$, is of less importance but its importance increases with increasing pressure.

Commonly $O_2(a^1\Delta_g)$ is suggested to be the main loss partner for $O^-$ ions in parallel plate reactors [18, 19], but our results indicate that the metastable oxygen molecule $O_2(a^1\Delta_g)$ plays a minor role in the loss of $O^-$ ions below 100 mTorr. The rate coefficients for detachment by collision of the oxygen ion $O^-$ with metastable oxygen molecules are taken from the measured values for the reaction $O^- + O_2(a^1\Delta_g) \longrightarrow$ products, given as $3.3 \times 10^{-17}$ m$^3$ s$^{-1}$ [41]. This recent measurement is considered to have an uncertainty of +100%/−50% and is about a factor of ten lower than previous measurements by Fehsenfeld *et al* in 1969 [42]. These previous measurements were accompanied by a factor of ten uncertainty. Consistent with earlier results, we assume one part producing $O_2^- + O$ and two parts producing $O_3 + e$. Thus

$$O^- + O_2(a^1\Delta_g) \longrightarrow O_2^- + O$$

$$k_{23} = 1.1 \times 10^{-17}(300/T_g)^{1/2} \text{ m}^3 \text{ s}^{-1}$$

and [41]

$$O^- + O_2(a^1\Delta_g) \longrightarrow O_3 + e$$

$$k_{33} = 2.2 \times 10^{-17}(300/T_g)^{1/2} \text{ m}^3 \text{ s}^{-1}.$$

The rate coefficient for the detachment by collision of the oxygen molecular ion $O_2^-$ with metastable oxygen molecules is [41]

$$O_2^- + O_2(a^1\Delta_g) \longrightarrow 2O_2 + e$$

$$k_{28} = 2.7 \times 10^{-17}(300/T_g)^{1/2} \text{ m}^3 \text{ s}^{-1}.$$

As seen in figure 8($b$) the effects of detachment by $O^-$ collisions with the metastable oxygen molecule $O_2(a^1\Delta_g)$ (reactions 23 and 33) are small in the pressure range usually applied in low-pressure high-density discharge, 1–20 mTorr. But the importance of these detachment processes increases with increasing pressure. At 300 mTorr recombination is still the dominating loss channel for $O^-$ ions but the detachment processes (reactions 23 and 33) account for a significant

fraction, roughly 1/3 of the loss of $O^-$ ions. Separately we investigated the effect of neglecting the detachment on the metastable molecular oxygen on the density of negative oxygen ions [28]. The $O^-$ density is a factor of 1.2 higher at 100 mTorr if the detachment (reaction 23 and 33) is neglected than if the detachment is included. The effect of neglecting the detachment on the $O^-$ negative ion density is smaller as we approach the pressure range commonly employed for high-density discharges and is a factor of 1.09 higher at 20 mTorr and negligible at 1 mTorr [28].

Recently, Hayashi and Kadota [43] reported on efficient production of $O^-$ in the afterglow of a low-pressure high-density oxygen plasma and explained the enhancement of the $O^-$ production by dissociative electron attachment from the excited metastable states of the oxygen molecule $O_2(A^3\Sigma_u^+, A'^3\Delta_u, c^1\Sigma_u^-)$ that are located 4–5 eV above the ground state [44]. We neglect these higher metastable states in this work.

### *3.5. The negative ion $O_2^-$*

The reaction rates $R$ for creation and destruction of the oxygen ion $O_2^-$ versus discharge pressure are shown in figures 9(*a*) and (*b*) respectively. The creation of $O_2^-$ is mainly through dissociative attachment of ozone $O_3$

$$e + O_3 \longrightarrow O(^3P) + O_2^- \qquad \text{(Reaction 31)}$$

with reaction rate $R_{31} = k_{31} n_e n_{O_3}$. The reaction rate coefficient for the dissociative attachment of ozone is estimated from the cross-section data of Senn *et al* [45]. Ozone is almost entirely created through detachment by the collision of $O^-$ with the metastable oxygen molecule $O_2(a^1\Delta_g)$ (reaction 33). The creation of $O_2^-$ is thus greatly influenced by this detachment process, and neglecting the detachment has a significant influence on the density of $O_2^-$; the density decreases by five orders of magnitude [28]. The creation of $O_2^-$ through detachment by the collision of $O^-$ with the metastable oxygen molecule $O_2(a^1\Delta_g)$ (reaction 23) and detachment by the collision of $O_3^-$ with ground-state oxygen atom $O(^3P)$ (reaction 37) are important processes at higher pressure but negligible at lower pressure (<10 mTorr).

At low pressure the $O_2^-$ ion is mainly lost through recombination

$$O_2^- + O^+ \longrightarrow O_2(^3\Sigma_g^-) + O(^3P) \qquad \text{(Reaction 25)}$$

with reaction rate $R_{25} = k_{25} n_{O_2^-} n_{O^+}$ while at higher pressure (>10 mTorr) charge transfer

$$O_2^- + O(^3P) \longrightarrow O_2(^3\Sigma_g^-) + O^- \qquad \text{(Reaction 29)}$$

with reaction rate $R_{29} = k_{29} n_{O_2^-} n_O$ is the main loss process. The non-dissociative three-body electron attachment to molecular oxygen in the ground-state $O_2(^3\Sigma_g^-)$ (reaction 26), detachment by collision of $O_2^-$ with the metastable oxygen molecule $O_2(a^1\Delta_g)$ (reaction 28) and ozone (reaction 41) and recombination involving $O_2^-$ and $O_2^+$ (reaction 24) play a smaller role in the loss of $O_2^-$ ions.

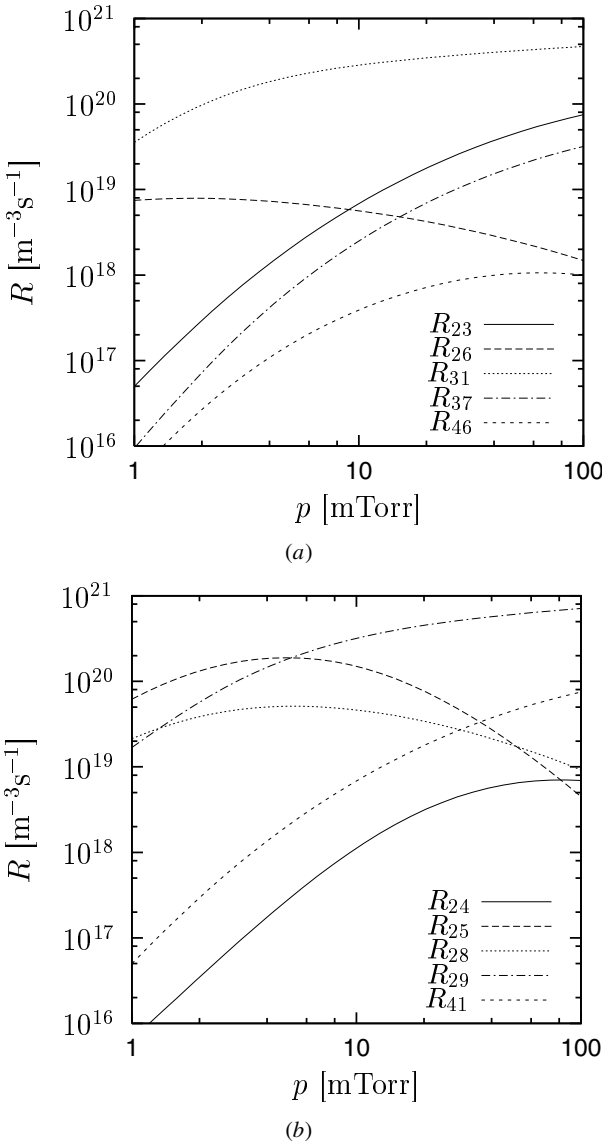


**Figure 9.** The reaction rates $R$ for (*a*) creation of the oxygen ion $O_2^-$ and (*b*) destruction of the oxygen ion $O_2^-$ versus discharge pressure at 500 W and a flow rate of 50 sccm for a cylindrical stainless steel chamber with $L = 7.6$ cm and $R = 15.2$ cm.

## 4. Conclusion

We applied a global (volume averaged) model to investigate the presence of negative ions in low-pressure high-density oxygen discharges. We formulate the normalized axial edge density for weakly electronegative discharge and multiple positive ion species. The negative oxygen ion $O^-$ is found to be the dominant negative ion in the discharge. The density of the negative ion $O_2^-$ is small and the density of the negative ion $O_3^-$ is negligible in the pressure range investigated. Dissociative attachments of the oxygen molecule in the ground-state $O_2(^3\Sigma_g^-)$ and the metastable oxygen molecule $O_2(a^1\Delta_g)$ are the dominant channels for creation of the negative oxygen ion $O^-$. At low pressure (<5 mTorr) recombination involving $O^-$ and $O^+$ ions is the dominating loss channel for $O^-$ ions. At higher pressure detachment on $O(^3P)$ becomes the main loss channel for the $O^-$ ion.

The creation of $O_2^-$ is mainly through dissociative attachment of ozone $O_3$. Ozone is almost entirely created through detachment by collision of $O^-$ with the metastable oxygen molecule $O_2(a^1\Delta_g)$. The creation of $O_2^-$ is thus greatly influenced by this detachment process and neglecting the detachment has significant influence on the density of $O_2^-$. At low pressure ($<10$ mTorr) the $O_2^-$ ion is mainly lost through recombination while, at higher pressure, charge transfer is the dominating loss process.

The metastable $O_2(a^1\Delta_g)$ molecule is thus of great importance in determining the negative ion density in an oxygen discharge at high pressures. However, at the low pressures (1–20 mTorr) commonly employed for high-density materials processing discharges, its role is minimal.

The model allows us to determine which reactions determine the discharge properties. In this work we investigate which reactions are important in the creation and destruction of negative oxygen ions. Many reactions included in this model have negligible influence on the discharge may not be worthwhile keeping in future modelling. Due to crude assumptions, including Maxwellian electron energy distribution, cross-section uncertainties, wall sticking coefficients and spatial uniformity, the global model is not meant to give accurate values of the plasma parameters. However, it can give an indication of how one parameter depends on another and which reactions among the species are important.

## Acknowledgments

This work was partially supported by the University of Iceland Research Fund, NSF Grant ECS-9820836, California Industries, and the State of California UC-SMART Program under contract 97-01.

## References

[1] Tolliver D L 1984 *VLSI Electronics: Microstructure Science* vol 8, ed N G Einspruch and D M Brown (Orlando, FL: Academic) pp 1–24
[2] Carl D A, Hess D W and Lieberman M A 1990 *J. Vac. Sci. Technol.* A **8** 2924
[3] Kitajima M, Kuroki H, Shinno H and Nakamura K G 1992 *Solid State Commun.* **83** 385
[4] Amemiya H, Yasuda N and Endou M 1994 *Plasma Chem. Plasma Proc.* **14** 209
[5] Heidenreich J E, Paraszczak J R, Moisan M and Sauve G 1988 *J. Vac. Sci. Technol.* B **6** 288
[6] Barnes M S, Forster J C and Keller J H 1993 *Appl. Phys. Lett.* **62** 2622
[7] Gudmundsson J T and Lieberman M A 1998 *Plasma Sources Sci. Technol.* **7** 1
[8] Gudmundsson J T 1999 *J. Phys. D: Appl. Phys.* **32** 798
[9] Mieno T, Kamo T, Hayashi D, Shoji T and Kadota K 1996 *Appl. Phys. Lett.* **69** 617
[10] Granier A, Nicolazo F, Vallée C, Goullet A, Turban G and Grolleau B 1997 *Plasma Sources Sci. Technol.* **6** 147
[11] Elíasson B and Kogelshatz U 1986 Basic data for modeling of electrical discharges in gases: Oxygen *Report KLR-11C* (Baden, CH5405: Brown Boveri Konzernforschung)
[12] Kossyi I A, Kostinsky A Y, Matveyev A A and Silakov V P 1992 *Plasma Sources Sci. Technol.* **1** 207
[13] Lieberman M A and Lichtenberg A J 1994 *Principles of Plasma Discharges and Materials Processing* (New York: Wiley) pp 251–6
[14] Lichtenberg A J, Vahedi V and Lieberman M A 1994 *J. Appl. Phys.* **75** 2339
[15] Chung T H 1999 *J. Korean Phys. Soc.* **34** 24
[16] Stoffels E, Stoffels W W, Vender D, Kando M, Kroessen G M W and de Hoog F J 1995 *Phys. Rev.* E **51** 2425
[17] Shibata M, Nakano N and Makabe T 1996 *J. Appl. Phys.* **80** 6142
[18] Buddemeier U 1997 *PhD Thesis* Ruhr-Universität Bochum
[19] Katsch H M, Sturm T, Quandt E and Döbele H F 2000 *Plasma Sources Sci. Technol.* **9** 323
[20] Franklin R N 2000 *J. Phys. D: Appl. Phys.* **33** 3009
[21] Ivanov V V, Klopovsky K K, Lopaev D V, Rakhimov A T and Rakhimova T V 1999 *IEEE Trans. Plasma Sci.* **27** 1279
[22] Lieberman M A and Gottscho R A 1994 *Physics of Thin Films* vol 18, ed M Francombe and J Vossen (New York: Academic) pp 1–119
[23] Lee C, Graves D B, Lieberman M A and Hess D W 1994 *J. Electrochem. Soc.* **141** 1546
[24] Lee C and Lieberman M A 1995 *J. Vac. Sci. Technol.* A **13** 368
[25] Gudmundsson J T, Kimura T and Lieberman M A 1999 *Plasma Sources Sci. Technol.* **8** 22
[26] Gudmundsson J T, Marakhtanov A M, Patel K K, Gopinath V P and Lieberman M A 2000 *J. Phys. D: Appl. Phys.* **33** 1323
[27] Patel K K 1998 *Master's Thesis* University of California at Berkeley
[28] Gudmundsson J T, Marakhtanov A M, Patel K K, Gopinath V P and Lieberman M A 2000 *J. Phys. D: Appl. Phys.* **33** 3010
[29] Rapp D and Briglia D 1965 *J. Chem. Phys.* **43** 1480
[30] Burrow P D 1973 *J. Chem. Phys.* **59** 4922
[31] Booth J P and Sadeghi N 1991 *J. Appl. Phys.* **70** 611
[32] Chantry P J 1987 *J. Appl. Phys.* **62** 1141
[33] Kouznetsov I G, Lichtenberg A J and Lieberman M A 1996 *Plasma Sources Sci. Technol.* **5** 662
[34] Hickman A P, Medikeri-Naphade M, Chapin C D and Huestis D L 1997 *Geophys. Res. Lett.* **24** 119
[35] Singh H, Coburn J W and Graves D B 2000 *J. Appl. Phys.* **88** 3748
[36] Greaves J C and Linnett J W 1959 *Trans. Faraday Soc.* **55** 1355
[37] Sharpless R L and Slanger T G 1989 *J. Chem. Phys.* **91** 7947
[38] Newman S M, Orr-Ewing A J, Newnham D A and Ballard J 2000 *J. Phys. Chem.* A **104** 9467
[39] Fuller N C M, Malyshev M V, Donnelly V M and Herman I P 2000 *Plasma Sources Sci. Technol.* **9** 116
[40] Tuszewski M 1996 *J. Appl. Phys.* **79** 8967
[41] Upschulte B L, Marinelli W J and Green D B 1994 *J. Phys. Chem.* **98** 837
[42] Fehsenfeld F C, Albritton D L, Burt J A and Schiff H I 1969 *Can. J. Chem.* **47** 1793
[43] Hayashi D and Kadota K 1998 *J. Appl. Phys.* **83** 697
[44] Hayashi D and Kadota K 1999 *Japan. J. Appl. Phys.* **38** 225
[45] Senn G, Skalny J D, Stamatovic A, Mason N J, Scheier P and Märk T D 1999 *Phys. Rev. Lett.* **82** 5028
[46] Lieberman M A and Lichtenberg A J 1994 *Principles of Plasma Discharges and Materials Processing* (New York: Wiley) pp 255–6
[47] Vejby-Christensen L, Kella D, Mathur D, Pedersen H B, Smidt H T and Andersen L H 1996 *Phys. Rev.* A **53** 2371
[48] Shimamori H and Fessenden R W 1981 *J. Chem. Phys.* **74** 453